Title

High-resolution PET detector design: modelling components of intrinsic spatial resolution

Journal

Physics in Medicine and Biology, 50(2)

ISSN

0031-9155

Authors

Stickel, Jennifer R

Cherry, Simon R

Publication Date

2005

DOI

10.1088/0031-9155/50/2/001

Peer reviewed

INSTITUTE OF PHYSICS PUBLISHING PHYSICS IN MEDICINE AND BIOLOGY

Phys. Med. Biol. **50** (2005) 179–195 doi:10.1088/0031-9155/50/2/001

High-resolution PET detector design: modelling components of intrinsic spatial resolution

Jennifer R Stickel and Simon R Cherry

Department of Biomedical Engineering, University of California—Davis, One Shields Avenue, Davis, CA 95616, USA

E-mail: jrstickel@ucdavis.edu and srcherry@ucdavis.edu

Received 19 September 2004, in final form 16 November 2004
Published 23 December 2004
Online at stacks.iop.org/PMB/50/179

Abstract

The development of dedicated small animal PET (positron emission tomography) scanners has led to significantly higher spatial resolution and comparable sensitivity to clinical scanners. However, it is not clear whether we are approaching the fundamental limit of spatial resolution. This work aims to understand what is currently limiting spatial resolution during data formation and collection and how to apply that knowledge to obtain the best possible resolution for small animal PET without sacrificing sensitivity. Monte Carlo simulations were performed of the interactions of a 511 keV photon in a variety of detector materials to evaluate the modulation transfer function of the materials. Positron range, non-colinearity and pixel size were modelled to determine the contribution of additional components of data formation and collection on the complete modulation transfer function of a PET system. These simulations are shown to predict the intrinsic detector resolution of current high resolution systems very well. They also show that current detectors are not limited by inter-crystal scatter. An intrinsic resolution of 0.5 mm can be achieved, but would require a detector with a pixel size of around 250 μm that can be read out unambiguously. It is shown that a range of different detector materials, both scintillators and semiconductors, can be used in these high-resolution detectors. While this design relies on thin ($\sim$3 mm) pieces of material, stacks of the material are shown to simultaneously provide spatial resolution near 0.5 mm and 60% efficiency. This work has shown that detectors with significantly better resolution and sensitivity can be developed for small animal PET applications.

1. Introduction

High spatial resolution and sensitivity in positron emission tomography (PET) are important goals, especially for small animal imaging applications. With the increased use of mouse models as a tool in biology, especially in the evaluation of new therapeutic strategies, there are many examples where the ability to visualize and accurately measure radiopharmaceutical accumulation in structures that have dimensions of a millimetre or less in size is important. Obvious examples include the early detection and evaluation of metastatic disease in mouse models of human cancer, and the study of cell trafficking dynamics in relation to the immune system and novel stem cell therapies. To achieve these goals requires the highest possible spatial resolution and sensitivity. While other considerations such as tracer specific activity and the concentration of the biologic target within the animal are also critical in determining whether a specific signal is measurable by PET, the range of applications for which small animal PET can be applied will clearly be dictated, to a large extent, by the resolution/sensitivity performance of the imaging system.

The sensitivity of most current animal PET scanners is in the range of 0.5–2.5% (Chatziioannou 2002) indicating that a large number of decays do not lead to recorded events. There are three major ways in which events are lost. First, one or both of the 511 keV photons may not intersect the detector system. This is remedied by designing PET systems with good solid angle coverage. Most current animal PET scanners have an average solid angle coverage of $<20\%$. Second, if a photon intersects a detector it may not interact in the detector. This requires that detectors have reasonable efficiency. Typical efficiencies are in the range of 20–70%, and of course depends on the detector material and its thickness. Finally, events can be lost if they fall outside the detector energy window. Tight energy windows (e.g. 350–650 keV) can reject a very significant fraction of events. It is therefore important to set energy thresholds that can capture all possible events that have not been subjected to resolution-degrading scatter in either the object or within the detector. In the low scatter environment of rodent imaging, it has been shown that it is not unreasonable to use a wide-open energy window (Yang *et al* 2004). The path towards much higher sensitivity animal PET systems, without increasing cost, is to design high-efficiency ($>60\%$) detectors with adequate depth of interaction resolution. They can be brought in close to the animal to reducing the detector area required per unit solid angle coverage. Using this approach, along with optimized energy selection, should yield system sensitivities in the range of 10–20%.

The other major issue in animal PET system design, and the primary focus of this study, is spatial resolution. The intrinsic spatial resolution of a PET detector is determined by many factors including positron decay physics, photon interaction physics, and detector material and geometry. It is not at all clear whether we are close to reaching the highest resolution possible for small animal PET. Most current systems are based on scintillators with individual detector elements as small as 0.8 to 1 mm in cross section (Tai *et al* 2003, Correia *et al* 1999, Miyaoka *et al* 2001). These detectors have reported resolutions ranging from 0.8 to 1.25 mm which can be directly related to the size of the detector elements with additional effects due to light production and collection, inter-crystal scatter and electronic multiplexing. More recently, solid state detectors have shown promise as room temperature direct detectors for nuclear medicine applications (Bennett *et al* 1998, Matherson *et al* 1998). Direct detection eliminates the complications related to scintillation light collection and detectors can also be manufactured with smaller pixelation than is readily achievable in scintillation crystals. However, their thickness is limited, and achieving adequate time resolution for PET applications is more challenging (Shao *et al* 2000, Giakos *et al* 1999). To determine if further significant gains can be made in PET detector resolution, and to identify

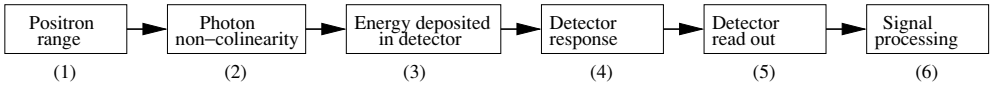

Figure 1. Linear system model of sources of resolution degradation in typical PET event generation.

possible detector configurations that can achieve such gains, it is necessary to understand how each of the factors identified above contributes to the overall resolution of a PET detector. Since these factors cannot easily be isolated and studied experimentally, Monte Carlo simulation and modelling is the most feasible approach for exploring the resolution limits and for predicting the performance of new detector designs.

In designing a high resolution PET detector, it is important to think of the chain of events that cause positioning uncertainty during event formation. Figure 1 shows a linear systems model of event generation starting with the production of the positron through the signal processing of the detector signals. The third box, energy deposition in the detector, is the first place where detector design can impact the spatial resolution. Detectors that minimize the distribution of energy deposition within the detector will produce the highest spatial resolution. The sources of positioning degradation can be understood by considering the fate of the 511 keV annihilation photons in the detector. The two main interactions that a 511 keV photon can undergo in detector materials are Compton scattering and photoelectric absorption. A Compton scattering interaction results in a scattered photon (energy range 170–511 keV) and a recoil electron (energy range 0–340 keV). Photoelectric absorption results in a photoelectron with an energy of 511 keV minus the binding energy of the electron, which ranges from a few keV at low Z to 60–90 keV for high Z elements such as Bi or Lu. Photoelectric interactions also result in characteristic x-rays (usually the K–L_{III} transition producing the $K_{\alpha 1}$ x-ray) with energies in the range from 50 keV to 80 keV. For both types of interactions, the electrons produced will deposit their energy locally. However, the x-ray produced in photoelectric absorption and the scattered photon from Compton interactions can, depending on the detector material and geometry, be absorbed some distance from the original interaction site. Alternatively, they may escape from the detector.

The first two boxes in figure 1 indicate sources of resolution loss due to the positron physics. Positron range effects are caused by the distance the positron travels prior to the annihilation and depends on the energy of the emitted positrons. The perpendicular distance from the location of the decaying atom to the line defined by the annihilation photons is the positron range blurring relevant for PET projection data. Because positrons are emitted with a range of energy and follow a tortuous path in tissue, the positron range is a highly non-Gaussian distribution as described by Derenzo (1979) and Levin and Hoffman (1999). Photon non-colinearity describes the deviation from 180° of the two annihilation photons. This is caused by the residual kinetic energy and momentum of the positron and electron at the time of annihilation, resulting in a small deviation from colinearity. This effect can be modelled as a simple Gaussian blurring function (Levin and Hoffman 1999). Scanner design can minimize non-colinearity by minimizing the separation between the detectors.

Several groups have used simulation to examine photon interactions in detector materials in the past. Examples include research to understand and minimize the scatter from one detector element to the next, usually with the focus on dense scintillator materials such as BGO (Levin *et al* 1997, Shao *et al* 1996, Burnham *et al* 1990, Thompson 1990). Other groups have studied energy discrimination or novel light collection schemes to improve spatial resolution (del Guerra *et al* 1998, Levin 2002, Correia *et al* 1999).

Our approach to this problem is to use Monte Carlo simulations and analytic blurring functions to characterize the limits imposed by positron physics, photon interactions

Table 1. Physical properties of detector materials used in the simulations.

Property	LSO	BGO	NaI(Tl)	Si	Ge	CZT
Effective atomic number	66	75	51	14	32	50
Density(g cm^{-2})	7.40	7.13	3.67	2.33	5.32	5.80
Linear attenuation coefficient (cm^{-1})	0.87	0.96	0.34	0.20	0.43	0.53
Photoelectric fraction	0.32	0.41	0.17	0.002	0.04	0.17
Compton fraction	0.63	0.54	0.79	0.99	0.93	0.79
Rayleigh fraction	0.05	0.05	0.04	0.008	0.03	0.04

and detector characteristics (i.e. detector material and dimension), and to predict the intrinsic detector resolution ultimately achievable by PET. We simulate and characterize the contributions from each of the first four boxes in figure 1. Table 1 shows the physical properties of the detector materials (scintillators and semiconductor materials) that we have chosen to investigate.

Our hypothesis is that to improve both resolution and sensitivity simultaneously, we will need to use all interacting events (no energy discrimination) and design detectors that are able to accurately identify the initial point of interaction within the detector. Using all events is not unreasonable in the case of small animal imaging, where the object scatter is low, and where in some detector designs, a large number of appropriately positioned events fall outside the traditional photopeak energy window (del Guerra *et al* 1998). For this reason, no energy windowing is utilized in the simulations that are reported. We also assume that the detector can accurately determine energy centroids, for example using individual detector elements with discrete read outs for each element. This would eliminate crosstalk, multiplexing and anger logic errors that would lead to event positioning errors (box 5 in figure 1). We also do not account for any resolution degradation introduced by the reconstruction algorithm or any other signal processing applied to the projection data (box 6 in figure 1).

We compare our simulation results to the results achieved in a number of existing high-resolution animal scanners, both to validate the simulations and to demonstrate that the effects due to boxes 5 and 6, at least in current detector systems, are small. Finally, we use the simulations to propose a detector design that can achieve high resolution and high efficiency as an example of how these results can be used to explore new detector designs for animal PET imaging.

2. Methods

2.1. Monte Carlo simulations of photon interactions

Monte Carlo simulations were performed using EGSnrcMP simulation code, which is a multi-purpose code for tracking both electrons and photons in matter (Kawrakow and Rogers 2001). In this work, photons refer to gamma-ray photons, not optical photons. Optical photons and light tracking are not considered in these simulations. The simulations consisted of one million 511 keV photons normally incident on the centre ($x = 0$, $y = 0$) of a semi-infinite slab of material with a defined thickness. Each interacting event was positioned at the calculated centre of mass of the deposited energy. This is the positioning approach underlying most current PET detector technology that is based on scintillation light sharing and/or electronic multiplexing techniques (Thompson 1990, Levin *et al* 1997). The six materials shown in table 1 were chosen for study, representing both scintillation materials that are currently used as indirect detector materials in PET systems and available semiconductor materials

Table 2. Detector material thickness as a function of total efficiency.

Efficiency (%)	LSO (cm)	BGO (cm)	NaI(Tl) (cm)	Si (cm)	Ge (cm)	CZT (cm)
20	0.27	0.25	0.69	1.11	0.53	0.45
60	1.12	1.01	2.82	4.57	2.18	1.83
95	3.65	3.31	9.22	14.95	7.13	5.98

that could be evaluated as direct detectors for PET applications. Simulations were carried out for all materials with matched total detector efficiencies of 20%, 60% and 95%. A 95% efficiency represents a detector that stops almost all incident photons but in which multiple interactions are common, a 60% efficiency (equivalent to ∼1 cm of LSO) represents the efficiency commonly found in small animal PET systems, and the 20% efficiency represents a detector that favours single-photon interactions. The thickness of a detector material required for each efficiency was calculated from the known densities and 511 keV photon cross sections of the material (Kawrakow and Rogers 2001, Berger *et al* 1999) and is shown in table 2. For each simulation run, list mode data were generated to give the location of each interaction, the type of each interaction and the energy deposited in each interaction. Compton and Rayleigh scattered photons, characteristic x-rays and any secondary radiation photons were all tracked until the energy dropped below 10 keV while Compton recoil electrons, photoelectrons, Auger electrons and any other secondary electrons were tracked until their energy dropped below 20 keV. Below these thresholds, all energy is assumed to be deposited locally.

2.2. Data analysis

Simulations of the detector materials with 20%, 60% and 95% efficiency were analysed by classifying the type(s) of interaction that each incident 511 keV photon underwent. A photon was classified as a 'C' event if it was only subject to a single Compton scattering interaction in which the scattered photon subsequently escaped from the material. The photon was classified as a 'PE' event if the first interaction was a photoelectric absorption. All other events (including multiple Compton scattering, Compton scattering followed by photoelectric absorption and events involving Rayleigh scattering plus either Compton scattering of photoelectric absorption) were classified as 'M' events to designate multiple interactions. All data were used in the analysis, irrespective of the total energy deposited, with the exception of events that only underwent Rayleigh interactions in the detector and therefore did not deposit any energy. The events were then processed into a 2D (x and y) histogram of the centre of mass of the deposited energy from each 511 keV photon. These histograms provide a visual representation of the spread of the centre of mass of the deposited energy from the initial photon direction through the material and can be thought of as representing the point spread function (PSF) of the detector material. Any spread of energy centre of mass away from the line of incidence (defined by $x = 0, y = 0$) leads to a degradation of the spatial resolution by introducing error in the determination of the location of the initial photon interaction. Because simulations are normalized for efficiency across different materials, these data provide a measure of spatial resolution degradation from photon interaction physics for a given total efficiency. We also computed the ratio of single interaction events (PE+C) to multiple interaction events (M) for each material and at each total efficiency, as the majority of the resolution degradation was shown to come from the 'M' events.

We chose to quantitatively characterize the detector PSF by using the modulation transfer function (MTF). The MTF was calculated by taking the 2D Fourier transform of the PSF

and then taking a radial profile through the resulting 2D frequency distribution. Because of the highly non-Gaussian nature of the PSF (due in large part to the exponential shape of the positron range blurring), characterizing these distributions with single numbers, such as the full-width at half-maximum (FWHM) or the root mean square (rms) deviation, does not provide a complete description of their effect. However, one figure of merit that we chose to employ was the total area under the MTF curve. This can be useful in comparing MTF curves that cross each other (Villafana 1978). MTFs were computed for all six materials at each of the three efficiencies.

2.3. Modelling positron physics and detector geometry

Three additional components from figure 1 were then modelled to provide a complete predicted detector response using the materials of interest. A pixelated detector was assumed and the detector geometric response modelled with pixel sizes of 1 mm, 500 μm and 100 μm. The pixels are modelled as ideal pixels with no gaps between pixels. This was implemented as a 2D triangular coincidence response function with a FWHM equal to one half the detector pixel size. Positron range was modelled as the sum of two exponential functions with parameters for ^{18}F given by Haber *et al* (1990). This model is based on the experimental data from Derenzo (1979). Finally, the photon non-colinearity was modelled as a Gaussian distribution with a FWHM $= 0.0022d$, where d is the system diameter (Levin and Hoffman 1999). This model is based on the experimental measurements from DeBenedetti *et al* (1950) and Colombino *et al* (1965). For small animal imaging applications, a practical minimum value of $d = 8$ cm was assumed. Both the positron range and non-colinearity were modelled as spherically symmetric functions in the 3D image space, projected onto the 2D detector plane.

2.4. Computing overall MTF and detector intrinsic resolution

The overall system MTF (in projection space) can be found by taking the product of the Fourier transforms of the individual blurring functions. This analysis allows comparison of the 'ideal intrinsic resolution' of different detector designs, limited purely by the physics of positron annihilation, photon interactions in the detector material, and the detector geometry, and excluding effects due to imperfections in the detector and its read out (for example light cross-talk, electronic cross-talk, light or charge production statistics and detector noise). The intrinsic resolution for an animal PET system as a function of pixel size was computed for LSO detectors of different efficiencies. To validate that the simulations presented here provide reasonable estimates of detector intrinsic resolution, this ideal resolution was compared to the intrinsic detector resolution actually measured and reported on a range of small animal PET systems.

3. Results and discussion

3.1. Effect of interaction type

Figure 2 shows the 2D histograms resulting from simulations of detector materials with 60% efficiency, with events grouped by interaction types. In all the histogram plots, the x and y axes are in centimetres and the intensity is shown on a log scale. The percentage of all interacting events contained in each category also are indicated. A number of clear trends emerge from these histograms. For all materials, the highest degree of blurring (mispositioning) comes from the multiple interaction ('M') events. This is because some energy is necessarily deposited at a site distant to the initial interaction point. It is also clear that for 60% efficient detectors, 'M'

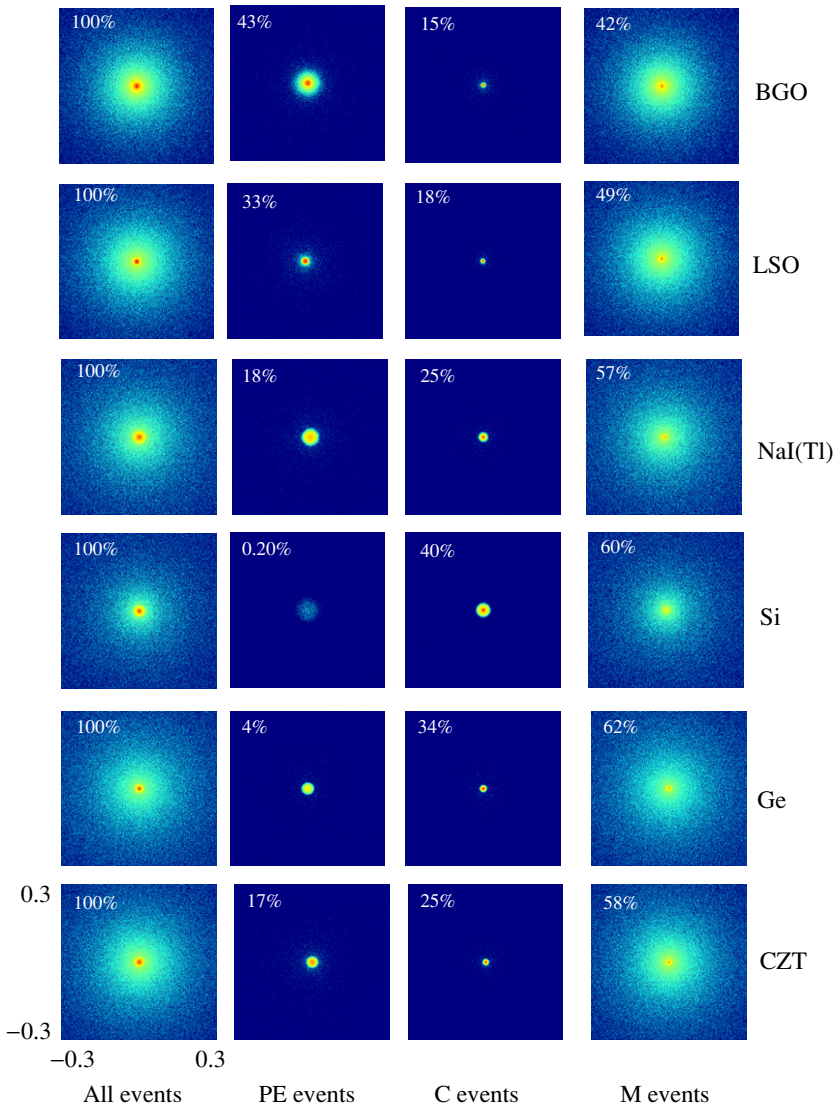

Figure 2. 2D histograms for all the materials as a function of event type. Matched efficiencies of 60% were used, the axes are in centimetres and the intensity is shown on a log scale.

events are very common, accounting for between 46% (BGO) and 62% (Ge) of the interacting events. The least positioning error occurs for single Compton ('C') events. The positioning error is less for 'C' events, as compared to 'PE' events, because of the differing energies of the by-products of the interactions. The recoil electron from a Compton interaction causes less blurring than the higher energy photoelectron and characteristic x-rays produced in a photoelectric absorption. Figure 2 also demonstrates that the lower Z materials have a higher proportion of 'C' events; however they also have a somewhat higher number of 'M' events. It is therefore not clear from these data which detector material gives the best results when all interacting events are utilized (left column of figure 2).

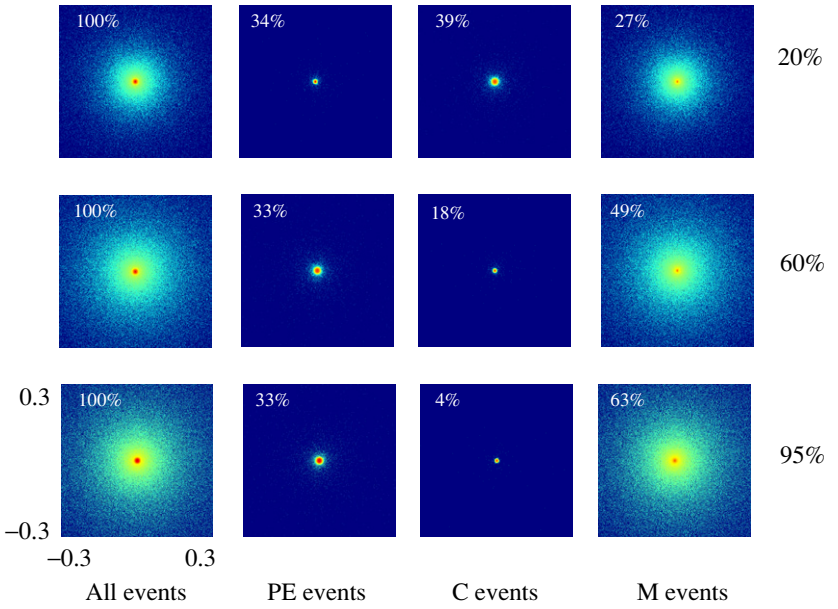

Figure 3. 2D histograms for LSO as a function of efficiency and event type. The M-type events lead to the greatest mispositioning, and the fraction of M-type events increases significantly with detector efficiency.

3.2. Effect of detection efficiency

Figure 3 shows the 2D histograms for the scintillator LSO as a function of detector efficiency and event type. In general, an increase in efficiency (and therefore in thickness) causes an increase in the positioning error. This is due to the increase in the number of events that undergo multiple interactions in the detector, compared with the number of single Compton interactions. The fraction of events interacting with a single photoelectric interaction is determined by the photoelectric cross section relative to the total cross section at 511 keV and is independent of detector thickness. However, the mispositioning of photoelectric events is reduced for low efficiencies, as the characteristic x-rays have a better chance of escaping without interaction. Figure 4 shows the 2D histograms for the semiconductor material CZT as a function of detector efficiency. At low efficiencies (thicknesses), there is little to choose between the two materials, but at higher efficiencies, the larger fraction of multiple interactions occurring in CZT is clearly a disadvantage relative to LSO. The data in figures 3 and 4 demonstrate that, independent of the material used, multiple interactions limit spatial resolution in 'thick' detectors. A reasonable goal in detector design is therefore to maximize the ratio of single to multiple detector interactions for a given total efficiency.

Figure 5 shows the ratio of singles to multiples interaction events for all six materials and three efficiencies. The ratio increases with increasing atomic number for total efficiencies of 60% and 95% as one would expect. However at 20% efficiency, some lower Z materials, for example Si, show a ratio comparable to that of high Z scintillators. A plot of the singles/multiples ratio as a function of atomic number and efficiency shows that low Z materials have a surprisingly high singles/multiples ratio for thicknesses that provide 20% efficiency (figure 6). This data suggest that if a high-efficiency detector module is to be built from a stack of lower efficiency 'slabs', it may not be advantageous to focus exclusively on high-Z detector materials.

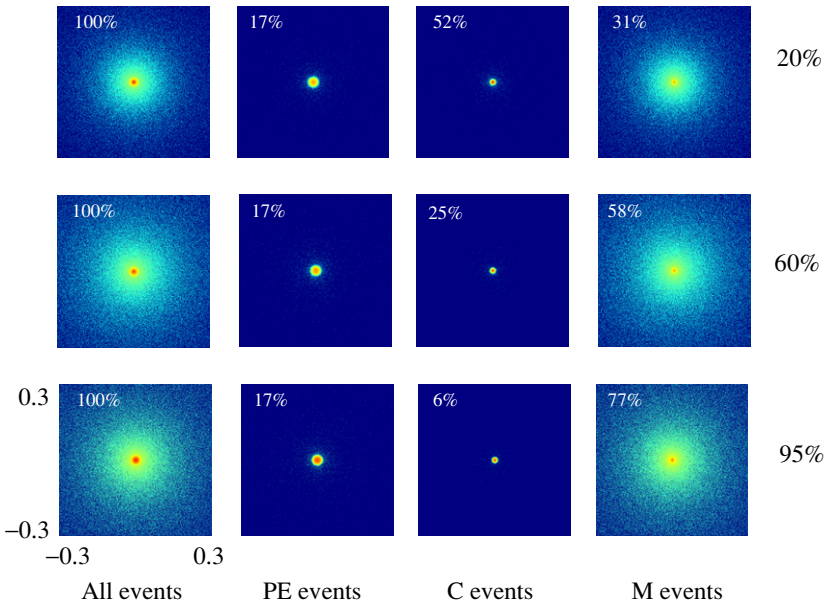

Figure 4. 2D histograms for CZT as a function of efficiency and event type.

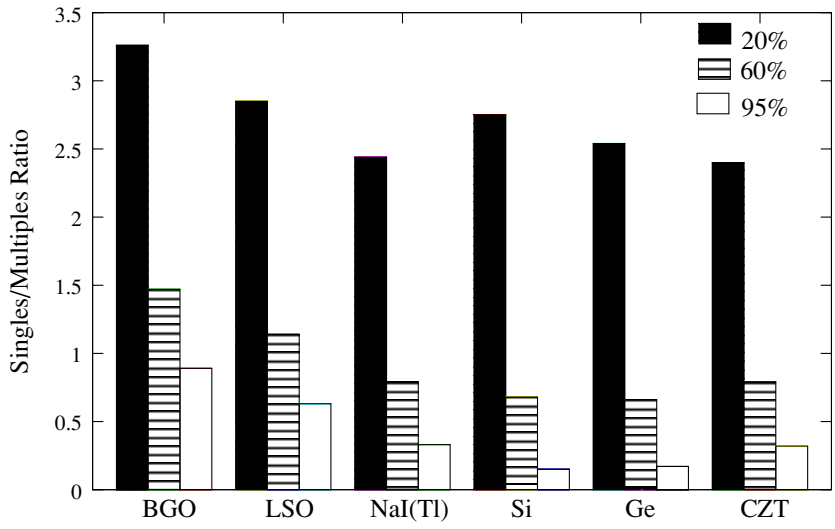

Figure 5. Bar chart showing the single/multiple interaction ratio for each of the detector materials at each efficiency.

3.3. MTF for different detector materials

Figure 7 shows the calculated MTFs for all detector materials and all efficiencies. The MTFs allow for a quantitative comparison between different materials. The curves generally show two components, a fairly rapid fall-off between 0 and 5 cm^{-1} primarily due to multiply scattered events, and a slower fall-off in the tails above 5 cm^{-1} that primarily corresponds to the single

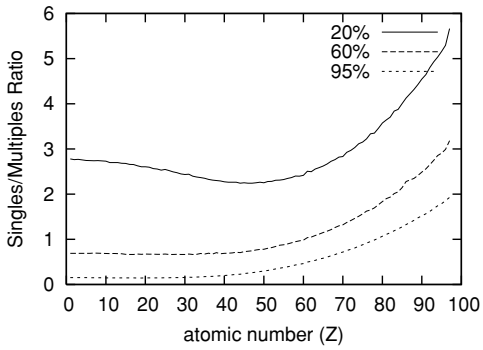

Figure 6. Plot of single/multiple ratio as a function of atomic number for all elements. For high efficiencies, this ratio increases monotonically with atomic number; however at 20% efficiency, the curve is no longer monotonic, with mid-Z elements leading to the lowest single/multiple interaction ratio.

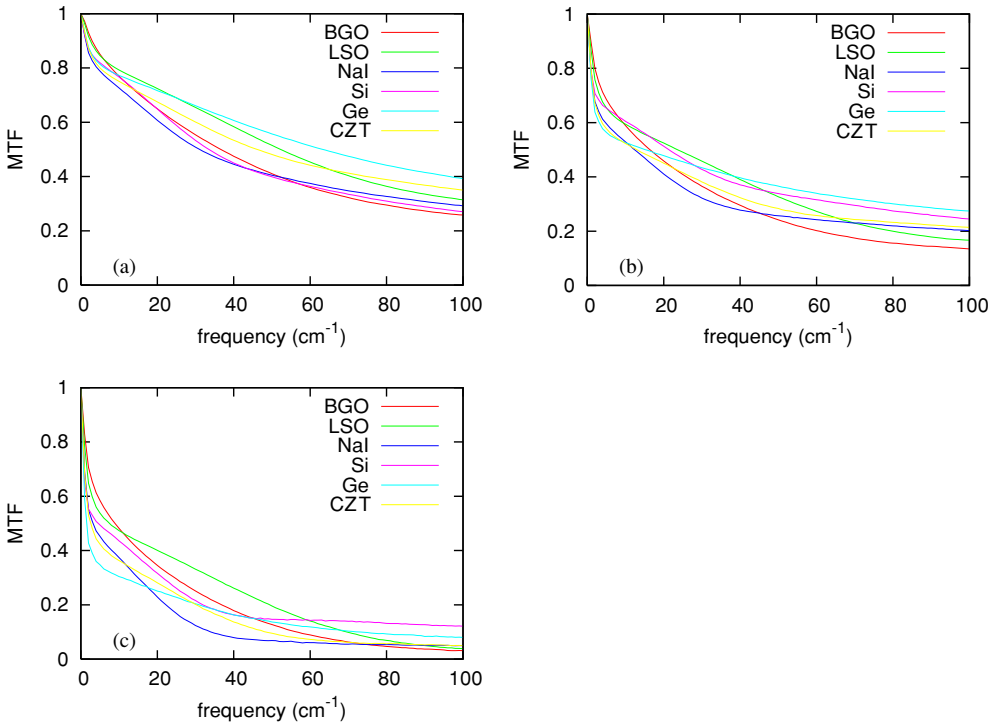

Figure 7. MTF plots for each material. Part (a) is for 20% efficiency, (b) is for 60% efficiency, and (c) is for 95% efficiency.

photoelectric and Compton interaction events. Figure 7 demonstrates that the MTFs of the 95% efficient curves are significantly depressed when compared to a 20% efficient detector. This indicates, not surprisingly, that the higher frequency information is better preserved in the thinner detectors. Figure 7 also shows that the MTF curves differ in shape for different materials and that the rank order of the curves changes both with efficiency and with spatial frequency. This implies that detector optimization will depend on the specific task and the

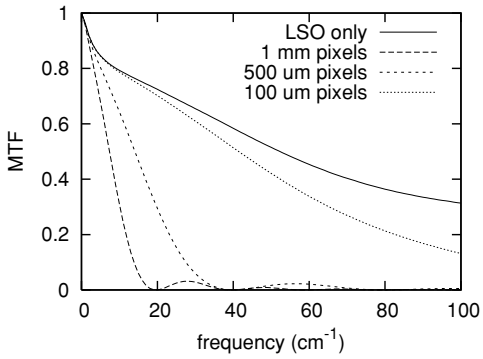

Figure 8. Effect of pixels sizes on the MTF for an LSO detector with 20% efficiency. Even very small pixels (100 μm) significantly degrade the MTF that is solely due to photon interactions in the detector material.

Table 3. Area under the MTF curves.

	BGO	LSO	NaI(Tl)	Si	Ge	CZT
20%	47.686	55.116	46.951	47.367	58.722	53.403
60%	31.658	37.082	32.133	39.566	39.872	34.331
95%	20.597	24.460	14.703	22.332	18.032	16.942

required spatial resolution and efficiency. To provide a figure of merit for the curves shown in figure 7, the area under the MTFs was calculated and is presented in table 3. A perfect MTF would yield a value of 100 on this scale. This simple figure of merit is useful when comparing MTFs that cross each other. It can be seen in table 3 that the largest MTF area varies with the detector efficiency. At 20% efficiency, Ge, LSO and CZT give the best MTFs while at 95% efficiency, LSO and Si give the best results. It is interesting to note that NaI(Tl) is one of the poorer materials at all efficiencies for this particular figure of merit.

3.4. Detector response modelling

In a real detector system, the measured detector response also will be subject to the geometric coincidence aperture function (due to the finite size of detector pixels or finite detector resolution). The detector element dimensions, modelled as a triangular response function with a base equal to the detector width, in conjunction with the photon interaction physics, will determine the best intrinsic spatial resolution that is achievable. The impact of the detector pixel size is shown in figure 8, in which, by way of example, the MTFs for a 20% efficient LSO detector are shown for pixel sizes of 100 μm, 500 μm and 1 mm. In this case, even the smallest pixel size leads to a significant degradation in the MTF at high frequencies, and the coincidence aperture function dominates the MTF for the larger pixel sizes. Figure 9 shows the MTF for all detector materials and for all three pixels sizes and detector efficiencies. These data clearly demonstrate that the pixel dimensions, not the photon interaction physics or detector material, dominate the detector MTF until the pixel size is reduced to a few hundred microns. These data indicate that it may be worth developing PET detectors with much smaller pixels than current state of the art systems (0.8 to 1 mm), as long as each pixel can be unambiguously decoded (i.e. no electronic or optical crosstalk) in the read out scheme. It also indicates, in the absence of considerations regarding crystal length and possible parallax errors, that the

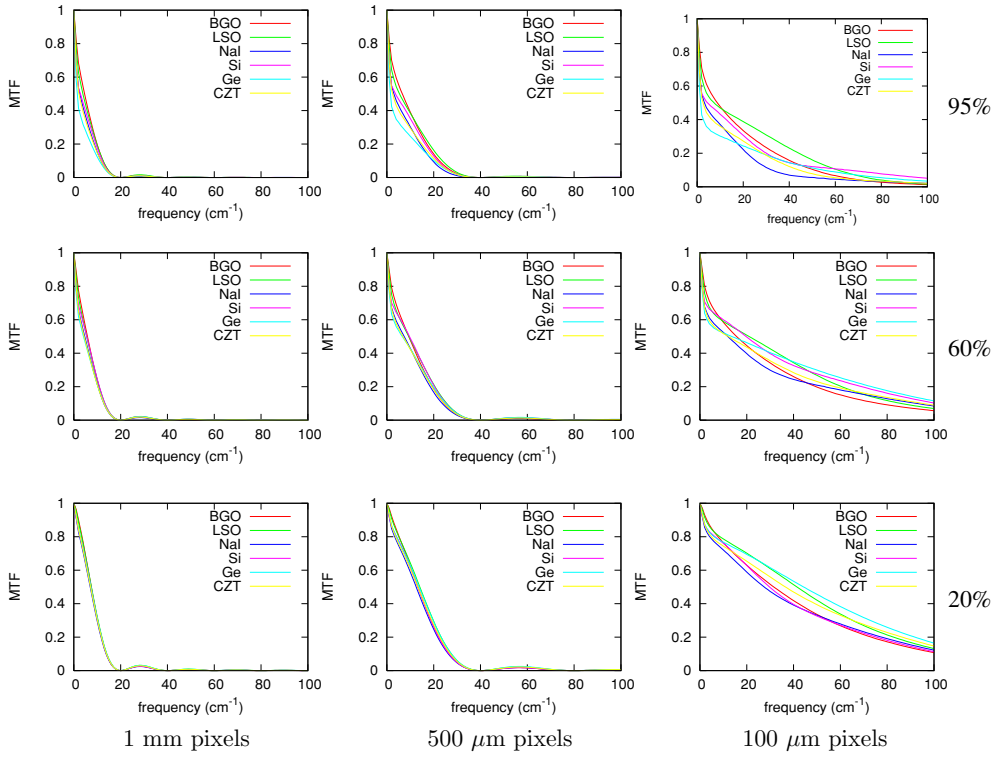

Figure 9. MTFs for all detector materials as a function of detector efficiency and pixel size.

detector material itself makes little difference to the resolution performance that would be realized when using pixels of around 1 mm in size.

3.5. Positron physics modelling

The discussion above ignores the deleterious effects of the physics of positron range and photon non-colinearity. To more completely model the overall detector response as presented in figure 1, we also computed the MTF due to positron range (^{18}F-labelled radiotracers) and non-colinearity (assuming a 8 cm diameter animal PET scanner). This represents the best possible case of a low-energy positron emitter and a small-bore scanner. The MTF components and total detector response are shown in figure 10 for a 500 μm pitch LSO detector. These data show that while material effects are important at very low frequencies ($<5\,\mathrm{cm}^{-1}$), the response at higher frequencies is dominated by positron physics and pixel size. Figure 11 shows a summary of the predicted detector response including positron annihilation physics for detectors for the various detector materials, efficiencies and pixel sizes. For 1 mm pixels, resolution is dominated by the pixel size. At 500 μm pixels and below, resolution is dominated by positron physics. The detector material plays a relatively minor role in determining resolution, with the impact of the detector material becoming more important with decreasing pixel size and increasing detector efficiency.

Figure 12 shows the FWHM and FWTM of the intrinsic detector resolution predicted for LSO PET detectors with different detector dimensions. The FWHM and FWTM are computed by taking the inverse Fourier transform of the curves in figure 11. A ^{18}F-labelled radiotracer

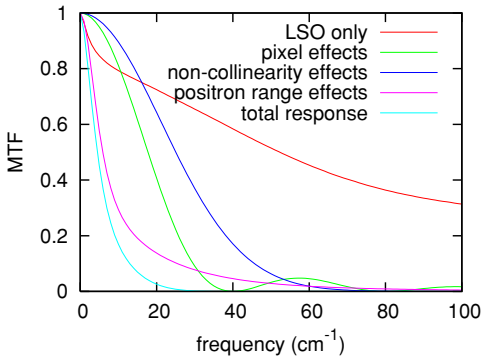

Figure 10. This graph indicates the different components of the total MTF. These data are for 20% efficient LSO detectors, separated by 8 cm and imaging a ^{18}F-labelled tracer.

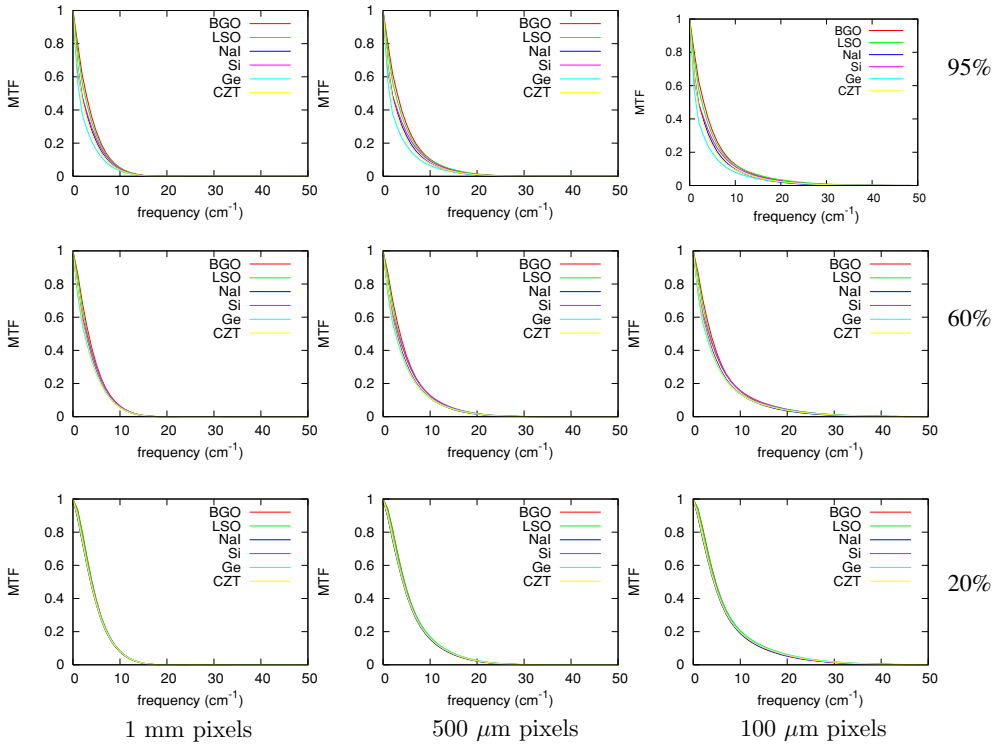

Figure 11. MTF for different detector materials, efficiencies and pixel size after modelling positron decay processes. Note that frequency axes only extend to 50 cm^{-1}.

and 8 cm detector separation are assumed. These data suggest that it is possible to achieve a limiting intrinsic resolution of around 500 μm, but only by using detector elements of 250 μm in size (or continuous detectors with equivalent intrinsic resolution). For discrete element detectors, it is further necessary that there is no significant multiplexing or decoding errors, such that each event is positioned in the detector where the energy centroid occurs.

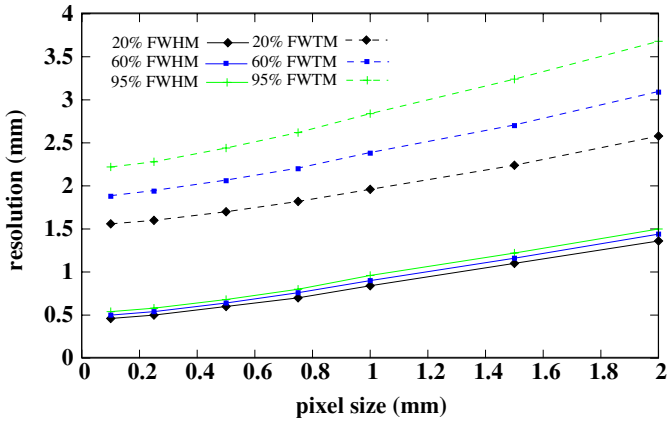

Figure 12. Plot of expected FWHM and FWTM as a function of detector pixel size with efficiencies of 20%, 60% and 95%. These plots assumed that the detectors are separated by 8 cm and that a ^{18}F-labelled probe is used.

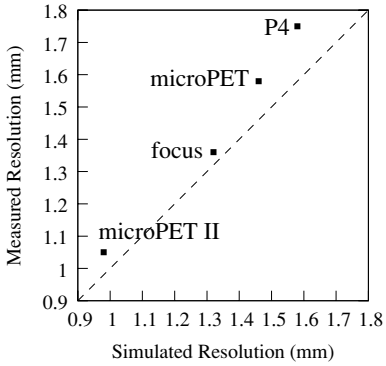

Figure 13. Plot of experimentally measured intrinsic detector resolution (FWHM) versus that predicted by our simulation for four animal PET scanners.

3.6. Verification of simulated data

To provide some measure of verification of these simulations, the predicted intrinsic spatial resolution was computed for a range of small animal PET detectors for which experimental data were also available (Tai *et al* 2003, 2001, Cherry *et al* 1997, LaForrest 2004). Figure 13 shows the comparison of the simulated and experimental results. The agreement is extremely good with all experimental results lying slightly above the line of identity, indicating some loss of resolution, likely due to the finite chance of mispositioning in these multiplexed detectors with finite light collection. It is encouraging to note however that this is a small effect, suggesting that these detectors perform close to the limits dictated by the detector geometry, photon interaction physics and positron physics effects.

4. Detector design

These results can be used to guide the design of new PET detectors with a goal of achieving very high spatial resolution and good efficiency. For example, figure 14 shows a potential direct semiconductor detector consisting of six 3 mm thick pixelated CZT detectors stacked

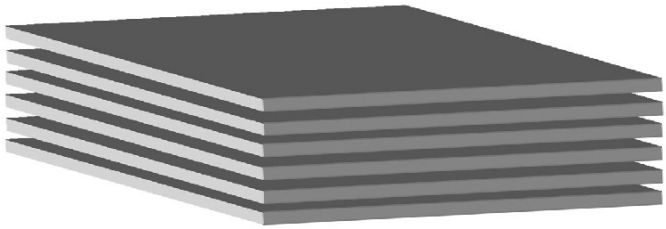

Figure 14. Potential future animal PET detector design based on a stack of 3 mm thick CZT detectors with pixel sizes of 250 μm.

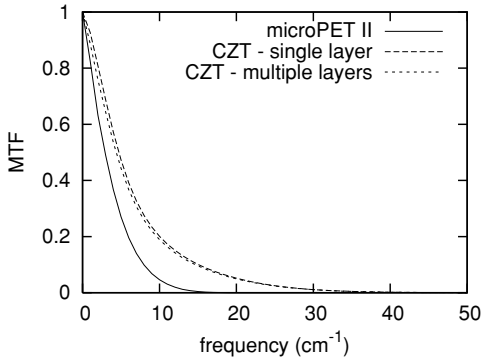

Figure 15. MTF plot for the multi-layered detector shown in figure 14, compared with a single-layered version of the same detector, and with the LSO detectors used in the microPET II scanner. This shows that a significant improvement in the MTF can be realized with the detector scheme shown, without any loss in efficiency compared with the LSO detector. There is negligible degradation in using a multi-layered approach versus a single-layered approach, showing that high-resolution, high-efficiency detectors can be built from stacks of lower efficiency units.

perpendicular to the direction of the incident photons. The total thickness of this detector would provide roughly the same stopping power as the LSO detectors used in the microPET II scanner (Tai *et al* 2003). If no events are rejected through energy thresholding, simulations indicate that the detector will have an efficiency of 61%. The advantage of using direct detection in a semiconductor is that small pixels can be readily created, and with appropriate electronics, interaction centroids accurately estimated. Even when small amounts of energy are deposited, such detectors have the potential to accurately locate events due to the large number of charge carriers produced (216 electron–hole pairs per keV deposited). The challenges related to this design include achieving adequate timing resolution from CZT (Giakos *et al* 1999, Parnham *et al* 2000), and the large number of electronics channels that have to be read out. Despite these challenges, it is still instructive to compare the performance of such a detector with a more traditional LSO-based scintillation detector.

When using multiple slabs in a detector, there is a probability that the photon may interact in more then one of the layers. The location of the first interaction can be based on several different schemes, including the signal-producing layer nearest the source, the signal-producing layer farthest from the source, a weighted energy of all interaction depths, or the layer with the largest energy deposition (Shao *et al* 1996). For this simple simulation, we positioned the event in the signal-producing layer nearest the source.

Figure 15 compares the MTFs for detectors from the microPET II scanner (0.955 mm pixels, 12.5 mm thick LSO, 15 cm detector separation), a single 3 mm slab of CZT and the

layered detector design described above. For the CZT detectors, the pixel pitch was assumed to be 250 μm, the detector separation was 8 cm and the positron source was ^{18}F. It can be seen that the MTF curves for both CZT detectors lie on top of each other indicating that there is no significant loss in resolution in comparing a multi-layer CZT detector over a single-layer detector. This is because the response of the detector is dominated by the pixel size and positron physics, and not scatter between the detector layers. It is predicted that this layered design would achieve a significantly higher spatial resolution than the microPET II detectors. Another advantage of the multi-layer design is that it naturally provides some level of depth of interaction information. Similar results are achieved using layered detectors consisting of 250 μm pixels of scintillator materials; however decoding such small crystals based on light-sharing techniques would be very difficult, and manufacturing these arrays of very small scintillator elements would be challenging.

5. Conclusion

This work has shown that Monte Carlo simulations, modelling of detector geometry and positron physics in conjunction with MTF analysis can be used to understand the components that determine intrinsic spatial resolution in PET detectors. The simulations presented here predict resolution responses of currently available systems well, with small discrepancies due to electronic and optical cross-talk as well as positioning logic uncertainty in real detectors.

The data shown here, as well as other simulation data not shown due to space constraints, indicate that inter-detector scatter is not the major limiting factor for current PET detectors. Positron range and pixel size dominate the resolution for small diameter (8 cm) PET systems.

The data also indicate that it is possible to obtain an intrinsic spatial resolution of around 0.5 mm using a detector pixel size of 250 μm or smaller. This can be achieved with a range of detector materials, including materials with a relatively low Z. However parallax (depth of interaction) effects must be considered if the detector design does not provide depth information and may become limiting depending on the thickness of the detectors and the system geometry.

Lastly, we have demonstrated how these data can be used to evaluate the intrinsic resolution and efficiency of new detector ideas, aiding in the design of a high-resolution detector for small animal PET. We show how a layered detector based on CZT can provide high spatial resolution, high efficiency, and through the layered approach also avoid resolution degradation due to depth of interaction effects. This design, and others like it that have been proposed (Levin 2002), have the potential to lead to significant improvements in the performance of small animal PET systems.

Acknowledgments

The authors would like to thank Jonathan Stickel for computer assistance and Guido Zavattini for technical discussions. Funding was provided by the Whitaker Foundation (JRS) and by NIH grant R01 EB00560.

References

Bennett P, Shah K S, Cirignano L, Klugerman M, Dmitriyev Y and Squillante M 1998 Multi-element CdZnTe detectors for gamma-ray detection and imaging *IEEE Trans. Nucl. Sci.* **45** 417–20

Berger M J, Hubbell J and Seltzer S M 1999 XCOM: photon cross section database *NIST Standard Reference Database 8*

Burnham C A, Elliott J T, Kaufman D E, Chesler D A, Correia J S and Brownell G L 1990 Materials for very high resolution PET detectors *IEEE EMBS Annu. Int. Conf.* **12** 0137–8

Chatziioannou A 2002 PET scanners dedicated to molecular imaging of small animals *Mol. Imaging Biol.* **4** 47–63

Cherry S *et al* 1997 MicroPET: a high resolution PET scanner for imaging small animals *IEEE Trans. Nucl. Sci.* **44** 1161–6

Colombino P, Fiscella B and Trossi L 1965 Study of postironium in water and ice from 22 to −144 degrees C by annihilation quanta measurements *Nuovo Cimento* **38** 707–23

Correia J A, Burnham C A, Kaufman D and Fischman A J 1999 Development of a small animal PET imaging device with resolution approaching 1 mm *IEEE Trans. Nucl. Sci.* **46** 631–5

DeBenedetti S, Cowan C, Konneker W and Primakoff H 1950 On the angular distribution of two-photon annihilation radiation *Phys. Rev.* **77** 205–12

del Guerra A, di Domenico G, Scandola M and Zavattini G 1998 High spatial resolution small animal YAP-PET *Nucl. Instrum. Methods* A **409** 537–41

Derenzo S 1979 Precision measurement of annihilation point spread distribution for medically important positron emitters *5th Int. Conf. of Positron Annihilation (Lake Yamanaka, Japan)* ed R Hasiguti and K Fujiwara pp 819–23

Giakos G *et al* 1999 Timing characteristics of a Cd $(1 - x)$ Zn (x) Te detector-based x-ray imaging system *IEEE Trans. Instrum. Meas.* **48** 909–14

Haber S F, Derenzo S E and Uber D 1990 Application of mathematical removal of positron range blurring in positron emission tomography *IEEE Trans. Nucl. Sci.* **37** 1293–9

Kawrakow I and Rogers D 2001 The EGSnrc Code System: Monte Carlo simulation of electron and photon transport *NRCC Report* PIRS-701, Ionizing Radiation Standards; National Research Council of Canada, Ottawa

LaForrest R 2004 Private communication

Levin C S 2002 Design of a high-resolution and high-sensitivity scintillation crystal array for PET with nearly complete light collection *IEEE Trans. Nucl. Sci.* I **49** 2236–43

Levin C S and Hoffman E J 1999 Calculation of positron range and its effect on the fundamental limit of positron emission tomography system spatial resolution *Phys. Med. Biol.* **44** 781–99

Levin C S, Tornai M P, Cherry S R, MacDonald L R and Hoffman E J 1997 Compton scatter and x-ray crosstalk and the use of very thin intercrystal septa in high-resolution PET detectors *IEEE Trans. Nucl. Sci.* **44** 218–24

Matherson K, Barber H, Barett H, Eskin J, Dereniak E, Marks D, Wollfenden J, Young E and Augustine F 1998 Progress in the development of large-area modular 64 × 64 CdZnTe imaging arrays for nuclear medicine *IEEE Trans. Nucl. Sci.* **45** 354–8

Miyaoka R S, Kohlmyer S G and Lewellen T K 2001 Performance characteristics of micro crystal element (MiCE) detectors *IEEE Trans. Nucl. Sci.* **48** 1403–7

Parnham K, Eissler E, Jovanovic S and Lynn K 2000 A study of the timing properties of Cd 0.9 Zn 0.1 Te (Available online at http://www.eVproducts.com/whitepapers.html)

Shao Y, Cherry S R, Siegel S and Silverman R W 1996 A study of inter-crystal scatter in small scintillator arrays designed for high resolution PET imaging *IEEE Trans. Nucl. Sci.* **43** 1938–44

Shao Y, Silverman R W, Farrell R, Cirignano L, Grazioso R, Shah K S, Visser G, Clajus M, Tumer T O and Cherry S R 2000 Design studies of a high resolution PET detector using APD arrays *IEEE Trans. Nucl. Sci.* **47** 1051–7

Tai Y C, Chatziioannou A, Siegel S, Young J, Newport D, Goble R N, Nutt R E and Cherry S R 2001 Performance evaluation of the microPET P4: a PET system dedicated to animal imaging *Phys. Med. Biol.* **46** 1845–62

Tai Y C, Chatziioannou A, Yang Y F, Silverman R W, Meadors K, Siegel S, Newport D, Stickel J and Cherry S 2003 MicroPET II: design, development and initial performance of an improved microPET scanner for small-animal imaging *Phys. Med. Biol.* **48** 1519–37

Thompson C J 1990 Effects of detector material and structure on PET spatial resolution and efficiency *IEEE Trans. Nucl. Sci.* **37** 718–24

Villafana T 1978 Advantages, limitations and signigicance of the modulation transfer function in radiologic practice *Current Problems in Diagnostic Radiology* vol 7 (Chicago, IL: Year Book Medical Publishers, Inc) pp 1–58

Yang Y, Tai Y C, Siegel S, Newport D F, Bai B, Li Q, Leahy R M and Cherry S R 2004 Optimization and performance evaluation of the microPET II scanner for *in vivo* small-animal imaging *Phys. Med. Biol.* **49** 2527–45